HHS Public Access

Author manuscript

Neuropharmacology. Author manuscript; available in PMC 2019 May 15.

Published in final edited form as:

Neuropharmacology. 2018 May 15; 134(Pt B): 259–271. doi:10.1016/j.neuropharm.2017.10.034.

MRI measurements of Blood-Brain Barrier function in dementia: A review of recent studies

Rajikha Raja, PhD, **Gary A. Rosenberg, MD**, and **Arvind Caprihan, PhD**

MIND research network, Albuquerque, New Mexico, and the Department of Neurology, University of New Mexico Health Sciences Center, Albuquerque, New Mexico

Abstract

Blood-brain barrier (BBB) separates the systemic circulation and the brain, regulating transport of most molecules to protect the brain microenvironment. Multiple structural and functional components preserve the integrity of the BBB. Several imaging modalities are available to study disruption of the BBB. However, the subtle changes in BBB leakage that occurs in vascular cognitive impairment and Alzheimer's disease have been less well studied. Dynamic contrast enhanced magnetic resonance imaging (DCE-MRI) is the most widely adopted non-invasive imaging technique for evaluating BBB breakdown. It is used as a significant marker for a wide variety of diseases with large permeability leaks, such as brain tumors and multiple sclerosis, to more subtle disruption in chronic vascular disease and dementia. DCE-MRI analysis of BBB includes both model-free parameters and quantitative parameters using pharmacokinetic modelling. We review MRI studies of BBB breakdown in dementia. The challenges in measuring subtle BBB changes and the state of the art techniques are initially examined. Subsequently, a systematic review comparing methodologies from recent in-vivo MRI studies is presented. Various factors related to subtle BBB permeability measurement such as DCE-MRI acquisition parameters, arterial input assessment, T_1 mapping and data analysis methods are reviewed with the focus on finding the optimal technique. Finally, the reported BBB permeability values in dementia are compared across different studies and across various brain regions. We conclude that reliable measurement of low-level BBB permeability across sites remains a difficult problem and a standardization of the methodology for both data acquisition and quantitative analysis is required.

Address Correspondence to: Rajikha Raja, PhD, MIND Research Network, 1101 Yale Blvd, Albuquerque, NM, 87106, rraja@mrn.org, Tel: 505-272-5028, FAX: 505-272-8002.

Disclosures

The patient images shown in this review were obtained as part of a study approved by the University of New Mexico Human Research Committee. All participants gave informed consent for all the study procedures. Patients were seen in the Neurology Clinics at the University of New Mexico and Veterans Administration Hospitals.

Contributions

Jillian Prestopnik, PhD was the study coordinator and helped recruit the patients. Dr. John Adair and Janice Knoefel were study neurologists, and performed neurological examinations along with Dr. Gary Rosenberg on the patients. Rajikha Raja, PhD reviewed the papers and wrote the first draft. Arvind Caprihan, PhD, was the NMR physicist who wrote the MRI sequences for the permeability study. Gary Rosenberg, MD, obtained the research funding. All authors participated in the writing of the manuscript.

Keywords

Dementia; Vascular cognitive impairment; Blood-brain barrier permeability; Dynamic contrast enhanced MRI

1. Introduction

Interest in the role of the blood-brain barrier (BBB) has surged in the past 10 years as an increasing number of neurological diseases have been linked to BBB disruption (Varatharaj and Galea, 2017; Zenaro et al., 2017) and the methods to measure permeability with magnetic resonance imaging (MRI) have become more available (Barnes et al., 2016; Heye et al., 2014; Heye et al., 2016; van de Haar et al., 2017). A major part of the expanded interest is the improvement in MRI instrumentation and the increased computer capacity for data analysis. The field has moved from the easily measured BBB damage in diseases with large permeability leaks, such as brain tumors and multiple sclerosis (MS), to more subtle disruption in chronic vascular disease and dementia. While there are a large number of research and review papers on the use of MRI permeability measurements in brain tumors and MS, relatively less has been written about the role of MRI permeability measurements in diseases with subtle blood vessel injury because of the problems encountered at low levels of leakage. Being able to detect lower levels of leakage will enable studies in patients with vascular cognitive impairment and dementia (VCID) and Alzheimer's disease (AD). This review will be focused on recently published studies of detection with MRI of low levels of permeability, including methodological challenges imposed by the small changes occurring in chronic diseases of the elderly that are confounded by changes in blood vessels with normal aging.

2. Background

2.1. Leakage across the blood brain barrier

The existence of a barrier restricting movement of molecules between the blood and the brain has been recognized for many years, the ability to quantitatively measure this transport in humans has only recently become available. The series of interfaces between the blood and brain tissues is referred to as the neurovascular unit (NVU) in order to emphasize that multiple cell types with different barrier properties are involved (Hawkins and Davis, 2005; Nelson et al., 2016). The first blood-brain interface is the endothelial cells that have tight junction proteins (TJPs), the next layer is formed by the basal lamina composed of extracellular matrix proteins, around the basal lamina are the astrocytic foot processes with the embedded pericytes. The NVU has high electrical resistance that restricts the passage of charged ions across the BBB except highly lipid soluble substances. In reality there is a small level of leakage across the NVU. While the interface between the blood and brain tissues is a relatively restrictive "barrier" to non-lipid molecules, in reality it has low permeability under normal conditions. In addition to TJPs, there are transport or carrier molecules that facilitate transport into the brain, and enzymes that degrade substances preventing their transport into brain. When there is a major breach of the BBB, such as occurring with brain tumors, stroke and multiple sclerosis, leakage of large proteins into the

brain tissue and cerebrospinal fluid (CSF) can be observed with contrast agents (CA) using either computed tomography (CT) or MRI. However, the pathological changes produced in the elderly with dementias involve much less dramatic changes, producing subtle leaks in the NVU. Such changes are best measured by MRI in clinically relevant timeframes.

2.2. Challenges in low permeability measurements in small vessel diseases

A low level of permeability is present in all cerebral vessels for non-lipid soluble molecules. Large molecules, such as albumin, move slowly into the CSF. Elevated albumin in the CSF suggests an opening in the BBB, making the albumin ratio of CSF to blood compartment a biomarker for opening of the BBB. Since the transport across the normal BBB is very slow, the time needed to detect a low level leak is relatively long. This results in the need for multiple measurements over a longer time than used for contrast-enhanced studies that are done clinically for diseases, such as, MS and brain tumors, where the leakage is at a much higher level.

Various review articles from the existing literature overlapped in partial forms with this topic of finding subtle BBB permeability in small vessel diseases (Bergamino et al., 2014; Farrall and Wardlaw, 2009; Heiss et al., 2016; Heye et al., 2014; Iadecola, 2015; Montagne et al., 2016a; Montagne et al., 2016b; Rosenberg, 2014; Snyder et al., 2015; van de Haar et al., 2015; Wardlaw et al., 2015). The studies on the similar topic were already reviewed in these articles up to June 2014. The information about those studies from the review articles is cross-referenced to include all the useful discussions. The other reviews have been written earlier and have not included data from more recent studies. By limiting our review to the past few years, we hoped to fill the gap with the older literature. In addition, we have compared the currently available methods, in terms of data acquisition, methods for permeability quantification, the application of these methods to dementia and small vessel cerebral vascular disease, and the differences in BBB leakage values between the research groups. This will allow various researchers to calibrate the transfer constants obtained by the different methods.

2.3. Comparison of methods used to measure BBB

Many methods have been used in BBB permeability studies. There are works reported based on postmortem investigations of BBB in dementia patients showing significant BBB damage (Tomimoto et al., 1996; Ujiie et al., 2003; Wisniewski and Kozlowski, 1982; Zipser et al., 2007). The major drawback of these studies is that they only report at the end stage of the disease. In animals, where removal of the brain is possible, investigators originally used dyes, such as Evans blue, injected into the blood to measure uptake into the brain. Radio-labelled isotopes of molecules that were transported quickly into the brain or those slowly taken up have provided more accurate measurements. ^{3}H-labelled water is rapidly taken across the BBB, making it a reference molecule when injected with slowly taken up compounds labelled with ^{14}C. A slowly taken up compound, such as ^{14}C-sucrose can be injected intravenously with the brain and blood sampled 20 minutes later; a single compartment transfer equation can be used to calculate the transfer assuming no back transport.

Albumin ratio was reported to be high in subjects with BBB damage. In-vivo studies were found in the literature using albumin ratio to investigate BBB in dementia (Algotsson and Winblad, 2007; Bowman et al., 2012; Frölich et al., 1991; Mecocci et al., 1991). Although these CSF studies showed higher albumin ratio in dementia, they lacked information about localization of leakage. CT and positron emission tomography (PET) provide methods to study the BBB permeability in humans. CT requires an iodinated CA and uses fairly high doses of x-rays. On the other hand, PET studies uses radioactive tracers to detect abnormalities. Commonly used PET tracer is ^{18}F-Fluorodeoxyglucose (FDG). Few of the studies have used PET for BBB assessment (Minoshima et al., 1997; Schlageter et al., 1987). PET studies are difficult to arrange due to the need to manufacture the isotope with a brief half-life. This makes MRI the most useful method for these studies.

3. Historical Background to Permeability Measurement

There have been several recent reviews on permeability measurement with MRI and we summarize the common concepts and terminology used (Heye et al., 2014; Sourbron and Buckley, 2013; Tofts et al., 1999b; van de Haar et al., 2015). The MRI methods for permeability measurement are based on the use of a paramagnetic compound as a CA, whose molecules can leak from the intravascular space to the interstitial space depending on the extent of BBB breakdown. The presence of paramagnetic molecules reduces the water relaxation times (T_1, T_2, and T_2^*), indirectly changing image intensity. The CA based methods have been divided in two groups: a) Dynamic susceptibility contrast enhanced MRI (DSC-MRI) based on T_2^* changes and b) Dynamic contrast enhanced MRI (DCE-MRI) based on T_1 images.

The paramagnetic agents typically used are Gadolinium (Gd)-based compounds, with the most common one being Gd-DTPA (gadopentate dimeglumine). The use of Gd-based CA has been restricted to patients with healthy renal function because of causing nephrogenic systemic fibrosis (Bleicher and Kanal, 2008). More recently it has been found that residual gadolinium is retained in patients even with normal renal function, raising further concerns about the use Gd as a contrast agent (Kanal and Tweedle, 2015). When a tissue comes in contact with paramagnetic Gd-based molecules, its relaxation rate ($R_1 = 1/T_1$ and $R_2^* = 1/T_2^*$) approximately increases from the baseline relaxation rates in proportion to the CA concentration. We have $\Delta R_1 = R_1 - R_{10} = r_1 CA_c$ and $\Delta R_2^* = R_2^* - R_{20}^* = r_2^* CA_c$, where R_{10} and R_{20}^* are baseline relaxation rates before the injection of CA, R_1 and R_2^* are the relaxation rates with the CA, and r_1 and r_2^* are the corresponding relaxivities. The T_2^* change depends not only on the local T_2, but it also depends on local magnetic field inhomogeneity. The susceptibility difference between the intravascular blood with CA and the tissue reduces field homogeneity, causing T_2^* to decrease. During the first pass of the CA, when its concentration is low and the CA has not leaked out to the extravascular space, r_2^* is higher than r_1, making DSC-MRI a more sensitive method for monitoring change than the DCE-MRI method. If the CA leaks out to the extra-vascular space, because of BBB breakdown, r_2^*

can drop because of reduced susceptibility differences between blood and tissue, making the dependence of T_2^* on CA concentration difficult to interpret. The current practice is to use DSC-MRI for cerebral blood flow (CBF) and cerebral blood volume (CBV) measurements, while DCE-MRI is used for making permeability measurements. Although with recent improvements in T_1/T_2^* weighted rapid sequences and better understanding of underlying physics, DCE-MRI has been used for CBF/CBV measurements (Sourbron et al., 2009) and DSC-MRI has been suggested for permeability measurement (Johnson et al., 2004).

In this review, our primary focus is on DCE-MRI methods for measuring low (subtle) permeability values. The flow diagram for such an experiment is shown in Figure 1. The data acquisition protocol consists of selecting the CA, its dosage, the choice of MRI experiment for T_1 measurement, and the number of baseline T_1 measurements before CA is injected. The T_1 calculation method depends on the MRI pulse sequence used for T_1 measurement and is variable across sites. As mentioned before the CA concentration is calculated based on the relaxivity value ($r_1 = 3.7 \pm 0.2\ \mathrm{mM^{-1}s^{-1}}$ for Gd-DTPA). The calculation of permeability related parameters depends on the tracer-kinetic model used for describing the CA leakage. The models and the notation used was standardized by Tofts (Tofts et al., 1999b), and a more modern description has been recently given (Sourbron and Buckley, 2013).

The extended Tofts model is given by

$$C_t(t) = K^{trans} \int_0^t e^{-k_{ep}(t-s)} C_p(s) ds + v_p C_p(t), \quad [1]$$

where $C_p(t)$ is the CA agent concentration in the plasma with volume fraction v_p, $C_t(t)$ is the CA concentration in the voxel under consideration, and s is a dummy variable in the integral. The voxel includes the extravascular extracellular space (EES) with a volume fraction v_e, other brain cells (yellow in Figure 2), plasma and the red blood cells (red in Figure 2). The rate constant for the CA to leak back into plasma from the EES space is $k_{ep} = K^{trans}/v_e$, and K^{trans} is volume-transfer constant across the BBB. K^{trans} is proportional to permeability, the parameter of interest. These parameters are described in Figure 2. In this review, we simply refer to K^{trans} as the permeability. $C_t(t)$ is CA concentration of the voxel where we want to calculate the permeability and $C_p(t)$ is the concentration in a voxel consisting of all blood. $C_p(t)$ is called the arterial input function (AIF) and is typically measured in common carotid artery or more typically in the sagittal sinus. A more appropriate nomenclature would have been vascular input function but to maintain consistency with the literature we call it AIF. The average concentration measured in a blood voxel $C_b(t)$ is related to $C_p(t)$ by hematocrit (H_{ct})

$$C_b(t) = (1 - H_{ct}) C_p(t). \quad [2]$$

Several simpler models can be obtained from Tofts extended model. If we put $v_p = 0$, we get the Tofts model and we get the Patlak model by putting $k_{ep} = 0$,

$$C_t(t) = K^{trans} \int_0^t C_p(s)ds + v_p C_p(t). \quad [3]$$

The Patlak model assumes that CA in the EES space does not leak back to intravascular space or move out of the voxel to neighboring voxels. Finally, if the permeability is zero we get

$$C_t(t) = v_p C_p(t). \quad [4]$$

In this case $C_t(t)$ is proportional to the CA concentration in the intravascular space. On comparing equations [1] or [3] to [4] we see that the permeability measurement depends on our ability to measure the accumulation of CA in the voxel that is due to its leakage across BBB. In other words, how accurately we can measure CA concentration above the intravascular concentration $v_p C_p(t)$. The volume fractions v_e and v_p are unitless, being defined as a ratio of two volumes, the units of K^{trans} and k_{ep} are min^{-1}. In the literature the units of K^{trans} are often written in units of ml/100g/min (for example, (Cramer and Larsson, 2014)). This depends on the CA concentration definition. If we assume that tissue density is approximately 1 g/ml, then 1 ml/100g/min is approximately equal to 0.01 min^{-1}. A subtle or low permeability (K^{trans}) is considered to be in the range of 10^{-4} to 10^{-3} min^{-1}, while permeability in tumors is of the order of 10^{-2} min^{-1}.

The baseline values of relaxation rates R_{10} (= $1/T_{10}$) and R_{20} (= $1/T_{20}$) across different brain regions affects the permeability calculations in different ways. An error in R_{10} measurement effects the CA concentration calculation. This leads to a bias error in K^{trans} calculation and can result in a negative calculated K^{trans}. On the other hand R_{20} does not appear directly in the model and because of the use of short echo times in the MRI data collection, its variation across the different brain regions does not have a significant effect on K^{trans} accuracy.

In this review we compare the differences across sites for each permeability measurement step indicated in Figure 1.

Methods based on the exchange of water across the BBB have been recently proposed (St Lawrence et al., 2012; Wang et al., 2007). These methods are attractive because they are based on exchange of water molecules across BBB and because they do not require the use of Gd contrast agent. The water molecule is smaller than a Gd molecule, and a subtle change in BBB permeability may be easier to detect by a water exchange rate change. By combining arterial spin labelling methods with diffusion it has been possible to separate the vasculer compartment with fast diffusion and an extra-vascular compartment with slow diffusion, and subsequently calculate the water exchange rate (St Lawrence et al., 2012). These methods are being developed, and as such we have not found their applications to dementia and

cerebral small vessel disease. This method has been validated in rats (Tiwari et al., 2017), and recently applied to a sleep apnea study (Palomares et al., 2015).

4. Materials and Methods

4.1. Search sources and selection criteria

We review the existing literature for quantification of subtle BBB permeability using imaging studies, specifically the dynamic contrast enhanced MRI (DCE-MRI). The literature up to May 2017 was searched using two sources, PubMed and Web of Science. Since the focus of this review is entirely on low BBB permeability measurements, we considered studies related to small vessel diseases, including all types of dementia and vascular cognitive impairment. In both PubMed and Web of Science, the following combination of terms were searched to be in title or abstract or keywords of article, "(blood-brain barrier OR BBB) AND (dementia OR mild stroke OR vascular cognitive impairment OR alzheimer OR binswanger OR small vessel disease OR AD OR BD OR mild cognitive impairment) AND (MRI OR magnetic resonance imaging).

4.2. Inclusion and exclusion criteria

The selected studies include all age groups and the disease groups as filtered by the search terms defined above. BBB permeability methodologies using DCE-MRI were included. The search results were refined manually to select the relevant articles of interest and also to discard the duplicates and the irrelevant ones. Moreover, the reference lists of those articles were checked carefully to include additional articles. The in-vivo studies assessing subtle BBB changes were included. Data from review articles pertaining to low BBB permeability measurements on the mentioned diseases were cross-referenced to include all possible studies. The flow diagram showing the selection of papers at each stage is shown in Figure 3.

4.3. Data extraction and analysis

We extracted the data from studies based on specific groups, (a) studies comparing quantitative measures of BBB permeability for disease conditions with subtle BBB permeability to healthy controls, (b) studies aimed at determining optimal BBB permeability measurement techniques and (c) review articles on the same topic. The data was extracted independently for each study included. Data related to in-vivo studies such as aim of the study, patient demographics, data acquisition protocol, CA type and dose, DCE-MRI analysis technique, quantitative parameters measured if any, major findings and final conclusion were tabulated to make them easy to compare. The studies which focused on identifying the optimal BBB permeability measurement technique were checked for data related to methodological aspects of DCE-MRI such as model selection, pulse sequences, mapping methods from T_1 to concentration curves, scanner drift, noise, spatial and temporal resolution, acquisition duration, arterial input function (AIF) and type of data analysis: region of interest (ROI) or a voxel based approach. Recommendations on the optimal values of these aspects were extracted from the articles.

The in-vivo studies were compared for quantitative metrics they provided for permeability measurements. In addition, the approach used in each study was analyzed, in terms of methodological factors to arrive at generic suggestions related to optimal methods for future studies.

5. Results of Literature Review

5.1. Categorization of studies reviewed

The articles resulted from electronic search were screened manually for full assessment inclusion. A total of thirty three articles were selected for review. The articles were categorized based on the aim of the work. The three different groups are: studies on measuring BBB permeability in diseased condition, studies aiming at determining optimal BBB permeability measurement techniques, and finally the review articles covering the same topic either partially or entirely. We found review articles including the relevant studies up to June 2014. The data provided in the review articles about those studies were cross-referenced to ensure full coverage of all the relevant studies.

5.2. Studies on measuring subtle BBB permeability in small vessel diseases

Eighteen in-vivo studies out of the total thirty-three were identified as studies with the primary aim of finding significant subtle BBB permeability changes in patients as compared to healthy controls. The patient groups across different studies had different disease groups. The studies (Munoz Maniega et al., 2017; Wardlaw et al., 2013; Wong et al., 2017; Zhang et al., 2017) reported on small vessel diseases and the associated BBB permeability metrics calculated using DCE-MRI. Two studies (Bronge and Wahlund, 2000; Shindo et al., 2005) related to dementia and three (Starr et al., 2009; van de Haar et al., 2016a; van de Haar et al., 2016b) reported on Alzheimer's disease. Three studies were on Binswanger's disease (Hanyu et al., 2002; Huisa et al., 2015; Rosenberg et al., 2015); two studies (Taheri et al., 2011a; Taheri et al., 2011b) related to VCI and one study (Wang et al., 2006) on MCI. The studies (Montagne et al., 2015; Starr et al., 2003) which reported on aging and diabetes were included in this review as they involved quantification of low level permeability changes in BBB.

The study details of eighteen in-vivo studies are summarized in Table 1. The sample size of most of the studies ranged from 25 to 100 including both patients and healthy controls. Only two studies (Munoz Maniega et al., 2017; Zhang et al., 2017) reported on a relatively larger population of around 100 samples and the population size of five studies (Montagne et al., 2015; Rosenberg et al., 2015; Taheri et al., 2011a; Taheri et al., 2011b; Wardlaw et al., 2013) ranged between 50 to 100. The mean age ranges of almost all studies were between 60 to 70. The MRI scanner field strengths used for the DCE-MRI acquisitions were 1.5T and 3T, except one study (Starr et al., 2003) on diabetes that used 1.9T scanner. Most widely adopted pulse sequence for DCE-MRI in the reported works is some variant of the gradient recalled echo (GRE) sequence. The more common method spoils the transverse magnetization at each step, reaches a steady spoiled state, and then acquires the imaging volume at different radio-frequency tip angles. These methods have been called SPGR/FLASH or FSPGR/Turbo-FLASH across different vendors. Other methods include saturation recovery GRE

methods (SRGRE), inversion recovery GRE methods (IRGRE), or the T1 mapping with partial inversion recovery method (TAPIR, (Shah et al., 2001)).

The different pulse sequences differ in the sensitivity and the temporal resolution for each T1 measurement, the brain volume coverage and spatial resolution. In the studies reviewed (Table 1) the temporal resolution varied from 0.5–5 minutes. The total experiment was in the order of 20–25 minutes, to allow for low level of leakage to be observed.

Gadolinium based CAs were typically used in all the studies with varying dosage levels from 0.025 mmol/kg (Taheri et al., 2011b) to 0.2 mmol/kg (Starr et al., 2003).

Table 2 summarizes the permeability values found across different research sites in healthy controls and Table 3 has the permeability values in patients across different research sites and with different disease groups. There are several interesting comparisons in Table 2 and 3. There are at least four major groups studying diseases with low levels of BBB permeability (Backes, Wardlaw, Zlokovic, and Rosenberg). Each group has been studying related but slightly different forms of small vessel disease, as summarized in Table 3. In the white matter for healthy controls, two out of three studies in Backes' group have $K^{trans} = 0.07 \times 10^{-3}$ min^{-1}, with the third study reports a value $K^{trans} = 0.97 \times 10^{-3}$ min^{-1}, which is more than 10 times higher. In Rosenberg's group two out of three studies have $K^{trans} = 1.5 \times 10^{-3}$ min^{-1}, with the third study reports $K^{trans} = 0.093 \times 10^{-3}$ min^{-1}, a value more than 10 times lower. The corresponding value for Zlokovic's group is $K^{trans} = 2.2 \times 10^{-3}$ min^{-1}. Indicating, that there is variability in permeability values measured at the same site and also across sites. Later in the discussion section we offer some reasons for these differences and what it means for reproducing these studies at different sites. The patient data in the white matter also shows similar trends across sites. Backes' group has the lowest values for K^{trans} in the white matter for patients, with Rosenberg's and Zlokovic's groups having similar higher values. We discuss later the causes and the implications of these differences.

5.3. DCE-MRI data analysis approaches

Both model free and pharmacokinetic modelling approaches were followed in the studies included in this systematic review. Semi-quantitative parameters derived from the signal enhancement curves and changes in T1 signal intensity were used to assess BBB dysfunction in the model free methods (Bronge and Wahlund, 2000; Hanyu et al., 2002; Munoz Maniega et al., 2017; Shindo et al., 2005; Starr et al., 2003; Starr et al., 2009; Wang et al., 2006; Wardlaw et al., 2013). In these studies, the parameters such as slope of the signal uptake curves, signal enhancement ratio and ratio of T1 changes were estimated for the ROIs. Differences in the estimated parameters between controls and patient groups or between normal and affected ROIs were analyzed statistically to arrive at BBB dysfunctionality conclusions. All the studies showed significant changes in BBB permeability associated with the corresponding disease, except one study (Bronge and Wahlund, 2000). Besides the advantages of model free analysis such as the elimination of AIF measurement and parameters like AUC are independent of injection protocols, the major challenges are that these parameters do not correlate physiologically and they are sensitive to variations between acquisition protocols.

Studies, which followed pharmacokinetic modelling approach, used Patlak model (Patlak and Blasberg, 1985) for the derivation of physiological parameters (Huisa et al., 2015; Montagne et al., 2015; Rosenberg et al., 2015; Taheri et al., 2011a; Taheri et al., 2011b; van de Haar et al., 2016a; van de Haar et al., 2016b; Wong et al., 2017; Zhang et al., 2017). The parameter K^{trans} indicating the BBB leakage rate was the widely used measure for permeability assessment (Huisa et al., 2015; Montagne et al., 2015; Rosenberg et al., 2015; Taheri et al., 2011a; Taheri et al., 2011b; van de Haar et al., 2016a; van de Haar et al., 2016b; Wong et al., 2017; Zhang et al., 2017). Yet another measure, v_p, the blood plasma volume fraction was also analyzed in a few studies (van de Haar et al., 2016a; van de Haar et al., 2016b; Wong et al., 2017; Zhang et al., 2017). Different methods for the mapping of T_1 to concentration curves and determination of arterial input function (AIF) were utilized. Variable flip angle, varying time delay and look-locker methods were a few of the widely used T_1 mapping MRI sequences. Individual specific measured AIFs were determined either from superior sagittal sinus or common carotid artery. The advantage of using model based approaches is that model parameters, such as K^{trans} can be directly related to BBB integrity, and show permeability differences between the normal and the diseased groups.

5.4. Studies on finding optimal DCE-MRI methodology for subtle BBB permeability

Five studies (Armitage et al., 2011; Barnes et al., 2016; Cramer and Larsson, 2014; Heye et al., 2016; van de Haar et al., 2017) reported on identifying the optimal DCE-MRI method for assessment of subtle BBB permeability. A large volume of reported literature is found in assessing the BBB permeability in acute disorders such as stroke and different tumors. These conditions involve a large variation in the permeability values and thus easily detected. Problems arise in cases of subtle permeability measurements owing to the requirement for a high level of accuracy and precision. Studies devoted to identifying accurate and precise DCE-MRI methodology for use in chronic diseases are gaining importance. This is because of the need to detect neuro-inflammatory diseases at an early stage, when the permeability is low, so that they can be treated.

Various factors ranging from acquisition protocol parameters to data analysis methods were quantitatively evaluated in these studies (Armitage et al., 2011; Barnes et al., 2016; Cramer and Larsson, 2014; Heye et al., 2016; van de Haar et al., 2017) for subtle BBB permeability measurements by introducing novel quality metrics and through in-vivo and simulation experiments. Recommendations on various methodological aspects were provided in these studies. The details of the studies along with the different factors considered and recommended solutions are summarized in Table 4. Selection of suitable pharmacokinetic model, acquisition duration, temporal resolution of the dynamic scans and influence of scanner drift are some of the factors analyzed. Two studies (Barnes et al., 2016; Heye et al., 2016) used specific metrics, contrast-to-noise ratio for K^{trans} (K-CNR) and Akaike information criterion (AIC) (Akaike, 1974) respectively, for assessing the model suitability. Simulation experiments were performed in these studies using different noise levels to evaluate the robustness of the methods. The pharmacokinetic model recommended for subtle BBB permeability measurement in three studies is Patlak model (Barnes et al., 2016; Cramer and Larsson, 2014; Heye et al., 2016). The acquisition duration and baseline scan duration recommendations are in the range of 10 to 30 minutes and 1 to 4 minutes (Barnes et al.,

2016; Cramer and Larsson, 2014). Scan time and sample size were analyzed with respect to different effect sizes in (van de Haar et al., 2017). The temporal resolution recommended being 1.25 seconds in (Cramer and Larsson, 2014) and less than 60 seconds in (Barnes et al., 2016). A recent analysis method improves the accuracy K^{trans} and v_p estimates by analyzing the first pass and the full data set iteratively with different models (Li et al., 2017). This method has not been applied to cerebral small vessel disease but the permeability values reported are in the range of subtle permeability range.

6. Discussion

Acquisition and Analysis Methods

We reviewed studies with the aim of identifying the optimal DCE-MRI method for the accurate measurement of subtle disorders of the BBB. We investigated a wide variety of factors influencing the measurements and also recommended optimal settings through experimental evaluations. Different pharmacokinetic models such as Tofts model (TM), extended TM, Patlak model, and two-compartment exchange model (Tofts et al., 1999a) were compared to find the optimal model. Patlak model was suggested to be the suitable model for subtle disorders. In the work reported by (Cramer and Larsson, 2014), Patlak model was suggested for low leakage rates with a threshold value of 0.3 ml/100g/min (approximately equal to 0.003 min^{-1}) which happens when the back diffusion is ignored. Moreover, increased accuracy and precision could be obtained by lengthening scan duration and increasing sampling frequency. Using the evaluation metric, K-CNR, Barnes and colleagues evaluated the precision of various models (Barnes et al., 2016). Based on K-CNR, Patlak showed superior precision due to the simplicity of the model involving only two free parameters as compared to other high complexity models. In alignment with the recommendations of these results, Heye and colleagues also favored the Patlak model based on the AIC rankings (Heye et al., 2016). AIC captures the goodness of fit and the complexity of the model through sum of squares differences and a number of free parameters, respectively. Even though the results suggested both Patlak and modified Tofts model to be adequate, Patlak was considered optimal because of fewer free parameters. This avoids overfitting errors which can occur when higher complexity models are used to fit the data in regions of low K^{trans} values, and the data does not support the more complex model.

In general, the acquisition duration followed for DCE-MRI protocol in various studies differed widely, with the recent methods collecting data for less than 30 minutes for measuring low permeability values. Low leakage rates are associated with subtle disorders. Longer scan times yield precise results of K^{trans} (Barnes et al., 2016; van de Haar et al., 2017) for low permeability values $< 2\times10^{-3}$ per minute. This is due to the increased number of measurements, which decreases the effect of noise and provides more time for the CA to extravasate to the extravascular tissue. In addition to longer scan times, acquiring a larger number of precontrast volumes, illustrating that increasing the baseline scan by 30 seconds leads to a 30% increase of K-CNR (Barnes et al., 2016). Since precontrast signal is required in the calculation of concentration curves, careful measurement of precontrast signal is needed for calculating an accurate concentration curve. Hence increasing precontrast time points increases the sensitivity of the study.

Dual temporal resolution data acquisition methods are attractive for permeability measurements (Jelescu et al., 2011; van de Haar et al., 2017). High temporal resolution is necessary to capture the contrast kinetics in tumor studies and with the added possibility of measuring cerebral blood flow. In these cases the spatial resolution is reduced. In cases of subtle permeability measurements, lower temporal resolution is preferred, in order to have better spatial resolution and coverage so that leakage rates could be measured across all brain structures. Barnes and colleagues (Barnes et al., 2016) demonstrated a threshold of 60 seconds as optimal sampling rate for subtle permeability measurements leading to higher K-CNR. Methods for measuring cerebral blood flow, cerebral blood volume, K_{trans} and v_p in white matter with one CA injection would be a major progress in DCE-MRI methods (Heye et al., 2016).

The influence of scanner drifts on the estimation of K^{trans} is negligible for large K^{trans} values. However, in case of low permeability regions, there is an increase in K^{trans} values with scanner drift (Heye et al., 2016). The effect of drift varies based on the tissue type and is specifically significant for CSF (Armitage et al., 2011). This makes drift correction using phantoms impossible in such cases. Scanner drift effects are more prominent in Patlak models due to its sensitivity towards lower contrast and hence affects inter-study comparisons (Barnes et al., 2016).

The two main deciding factors to increase the accuracy of BBB permeability measurements using pharmacokinetic models are the estimation of concentration curves from T_1 signal intensities and the determination of AIF. The most commonly used methods for T_1 mapping are the variable flip angle (Brookes et al., 1999) and variable saturation time delay methods (Larsson et al., 1988). These methods were developed to calculate the pre-contrast longitudinal relaxation time T_{10} which is required for the mapping of signal enhancement to CA concentration. The importance of accurate estimation of T_{10} was shown by (Schabel and Parker, 2008). In the SPGR methods, the flip angle errors, the error between the actual and operator defined flip angles influences the calculated T_1 values. Alternative approaches such as Look-Locker based methods (Shah et al., 2001), and DESPOT1-HIFI (Deoni, 2007) overcome such errors. The step of AIF determination also plays a critical role in the estimation of kinetic parameters. For subtle permeability regimes, individual AIFs extracted from superior sagittal sinus or common carotid artery were used in the existing works. The vascular input function extracted from superior sagittal sinus was unaffected by partial volume and inflow artefacts (Lavini and Verhoeff, 2010) and it can be easily identified.

The method of reporting the permeability values in the literature also differs across groups. The permeability can be a calculated over a region-of-interest or for every voxel in the image. The difficulty in obtaining trustworthy estimates of low permeability is well illustrated by the histogram of permeability values across the image (van de Haar et al., 2017). A large number of voxels have a negative permeability. We have also noticed this in our studies. In their study they have proposed mirroring the negative permeability histogram to compensate the positive section of the histogram. The statistical relevance of this step is not clear but it does suggest that negative calculated permeability values have to be dealt with. An alternative approach used by our group is to use the AIC approach to select an appropriate model with one choice being the simple model of zero permeability (Eq. 4). If

the data is noisy then this model explains the data equally well based on the AIC criterion and we estimate $K^{trans} = 0$. Another step we take is to report permeability values above a threshold of 0.003 min^{-1}. The value of the threshold was chosen on the basis of receiver operating characteristic (ROC) analysis which best separated healthy controls from our patients. This leads to lower values of permeability not being reported but does give greater confidence on higher permeability values indicating regions of BBB breakdown. The choice of the threshold will depend on the method of data acquisition and the disease being studied. The appropriate threshold value will vary from site to site because of differences in methods used across sites. A review of the available software tools and a software code written in MATLAB is available for processing DCE-MRI data, which offers the flexibility of experimenting with different tracer-kinetic models (Barnes et al., 2015). The software does appear to be focused on the SPGR techniques for T1 mapping.

In practice, the measurement of permeability in white matter has several advantages over those in the cortex, primarily due to the large amount of white matter and the proximity of the cortex to the CSF space, allowing the CA to obscure the cortical readings during prolonged scans. In this review, we showed several examples of the region-specific increase in permeability around the WMHs and in the normal appearing white matter. While white matter in the vascular cognitive impairment patients shows marked increases, there is low permeability in the white matter in Alzheimer's disease. The reason for this remains to be more fully studied. Finally, permeability measurements tend to fluctuate over time in a manner similar to that seen with relapsing and remitting multiple sclerosis. While these differences will aid in classifying patients, the fluctuation over time will interfere with the use of permeability as a measure of the success of therapies.

Vascular cognitive impairment

A number of investigators have used the MRI with the Patlak plot method to measure the low levels of cerebral permeability in chronic vascular diseases. White matter permeability measurements are facilitated by the large volume of contiguous tissue in the white matter tracts. Permeability in the normal-appearing white matter (absence of white matter hyperintensity in FLAIR) has low-level leakage of CA probably due to the minimal transport through endothelial cells and tight junctions. In addition, there are no studies of the stability of the MRI BBB measurement over time. A comparison of Tables 2 and 3 indicates that the permeability values vary across sites and also within a site for white matter in controls. This shows that there is a bias in permeability values being reported across sites. This bias exists because of different amounts of Gd-dosage, different methods being used for data acquisition, and different methods of processing the data and finally different permeability measures are reported in the literature. An example is the difference in methods of post-processing the MRI data in Backes' group and Rosenberg's group. In Backes' group the negative permeability values are reflected over to the positive side to compensate for negative values, while in the Rosenberg's group the permeability is only calculated above a threshold of 0.003 min^{-1}. Although the threshold was chosen by careful consideration to distinguish the calculated permeability between patients and controls, the permeability values are biased to higher values. The permeability differences observed between healthy

controls and patients at any one site are acceptable, but it is very difficult to compare studies across sites.

Table 5 summarizes the effect size ($(\mu_{patient} - \mu_{control}) / s_{pooled}$ between patients and controls for studies where the mean permeability and the standard deviation was available. The effect size ranges from 0.07 to 1.8. Three of the studies (Montagne et al., 2015; van de Haar et al., 2016b; van de Haar et al., 2017) shows effect sizes below medium value of 0.5 (Cohen, 1992), while the remaining five studies (Taheri et al., 2011a; Taheri et al., 2011b; van de Haar et al., 2016a; van de Haar et al., 2016b; Zhang et al., 2017) reveals effect size values above medium range. Higher effect sizes were obtained for the Rosenberg group (Taheri et al., 2011a; Taheri et al., 2011b). The higher values in the Rosenberg's group are probably because of the threshold method of reporting the permeability values, which emphasized the differences between the controls and the patients. On comparing the effect sizes within the study groups, Backes group (van de Haar et al., 2016a; van de Haar et al., 2016b; van de Haar et al., 2017; Zhang et al., 2017) showed large variations in effect sizes across different studies. This is possibly due to the difference in the disease groups and sample sizes between these studies.

Leakage of Gadolinium into the white matter in patients with vascular cognitive impairment has been demonstrated by a number of investigators. The disruption of the BBB in chronic vascular disease has been linked with hypoxia induced inflammation. One potential scenario involves chronic changes in the blood vessels secondary to long-standing elevated blood pressure. This results in narrowing of the vessel lumen, restricting cerebral blood flow, and producing hypoxia. This hypoxia is most likely intermittent, such as occurs in sleep apnea, rather than long-term as seen with cerebral infarction. This is supported by animal studies in which the levels of oxygen in hypertensive rats are directly measured with electron paramagnetic resonance (EPR) (Weaver et al., 2014), and by studies in humans that have found hypoxia inducible factor in the brains of patients with vascular dementia (Fernando et al., 2006). Other factors may be involved. A recent study showed that stiffening of the aorta which is transmitted to the small arteries of the brain, increases free water as measured with diffusion tensor imaging (Maillard et al., 2017).

When the white matter is abnormal there are variable changes in the permeability. In white matter regions with gliosis, as shown by white matter hyper-intensities (WMH), the permeability is very low. However, at the edges of the WMH, the penumbra regions, there is an increase in leakage, suggesting this is an active site of on-going damage. More importantly, permeability changes are found in the so-called normal-appearing white matter (NAWM) (Huisa et al., 2015). This is interesting and suggests that there may be low-level of on-going damage even in the regions that appear normal on FLAIR MRI. A similar finding has been made using the diffusion measurements, which identify changes in white matter regions with normal signal on FLAIR (Maillard et al., 2013).

Permeability is increased in the deep white matter in patients with VCID. While FLAIR MRI indicates regions with WMH, these regions may have normal integrity as shown by proton-magnetic resonance spectroscopy (Brooks et al., 1997). However, the regions lacking FLAIR increased signal may show abnormal structural integrity on DTI, which has been

referred to as abnormal normal-appearing white matter, which is a paradoxical designation. In an earlier study by our group, we found markedly reduced permeability inside the white matter hyper-intensities with the majority of the increased permeability in the “penumbra” around the white matter hyper-intensities, and the remainder in normal-appearing white matter (Figure 4) adapted from (Huisa et al., 2015)). A similar finding has been made using the diffusion measurements, which identify changes in white matter regions with normal signal on FLAIR (Maillard et al., 2013). Regions of elevated permeability were observed in the periventricular tissues, the deep white matter of the corpus callosum, and at the junction of the gray and white matter. A similar finding has been made using the diffusion measurements, which identify changes in white matter regions with normal signal on FLAIR (Maillard et al., 2013).

Alzheimer’s disease

Studies done in the gray matter of the hippocampus in patients with early Alzheimer’s disease suggest that the BBB is open (Montagne et al., 2015). These investigators found permeability changes in the hippocampus, but not in the white matter. Patients with cerebral amyloid angiopathy have microbleeds suggesting increased permeability, but measurements of K^{trans} have not been made with MRI in humans. Qualitative observations of contrast-enhancing lesions in patients with cerebral amyloid angiopathy have been reported (Hartz et al., 2012). This is an area that is in need of further study in both hypertensive and non-hypertensive population.

Measurements in cortical gray matter are challenging because the cortex is a thin layer of gray matter contiguous to the CSF with the added complication of tortuous sulci that fold into the white matter. One way to obtain measurements in the gray matter is to perform shorter uptake studies. Another strategy is to obtain permeability measurements in the deep gray matter structures such as the basal ganglia and hippocampus.

7. Conclusion

Measurement of BBB disruption at its early stages is important in many neurological disorders. This requires measuring low permeability values and we have seen this is a difficult challenge for MRI methods based on Gd-based CAs. In order for these methods to be uniformly adopted across different sites it is necessary that current advances in imaging technology be incorporated in the methods and collaboratively a uniform protocol is proposed. The challenges are at each step in the process described by Figure 1. The Gd-dosage is important because we are measuring low permeability changes and sacrificing contrast by using low-dosage may not be advisable. Current T_1 measurement methods provide more rapid methods for monitoring T_1 change and can provide whole brain coverage, or alternatively coverage of a slab at a higher spatial resolution. We feel a common method for T1 mapping across sites will be beneficial. Majority of the sites use some form of SPGR but agreeing on a more uniform protocol will help. Some groups are presenting dual temporal resolution acquisition methods. These methods combine a low spatial resolution and high temporal resolution images during the first pass images which are then followed by higher spatial resolution and low temporal resolution images to capture low

values of CA leakage. These methods are attractive because they may provide better accuracy in gray matter by taking into account higher perfusion in gray matter. In regions of low permeability, the dual resolution method may have the advantage that during the first pass of the CA, the signal enhancement in the white matter is totally dependent on the intravascular compartment, because the minimal leakage has occurred, and we could get good estimates of plasma volume fraction v_p. The current MRI methods for BBB permeability measurement are all based on using Gd-based compounds as CA. The Gd-based compounds have nephron-toxicity and are not advisable to use in some cases. An alternative MRI method based on increased water diffusion across the BBB can be very attractive if developed. The analysis methods need harmonization, which includes looking at changes during the first pass of the bolus and understanding the contrast behavior in the gray matter and the CSF.

Measuring low values of BBB permeability in white-matter by MRI remains a difficult problem and requires a joint community effort to come up with a robust method that can be implemented uniformly across sites, and which take into consideration recent advances in MRI hardware and software.

Acknowledgments

Funding

The study was funded by grants from the NIH RO1 NS 052305 and the US-Israeli Binational Research Foundation to GAR, and the National Center for Research Resources and the Nation al Center for Advancing Translational Sciences of the NIH through Grant Number 8UL1TR000041, UNM Clinical and Translational Science Center.

References

Akaike H. A new look at the statistical model identification. IEEE transactions on automatic control. 1974; 19:716–723.

Algotsson A, Winblad B. The integrity of the blood–brain barrier in Alzheimer's disease. Acta Neurol Scand. 2007; 115:403–408. [PubMed: 17511849]

Armitage PA, Farrall AJ, Carpenter TK, Doubal FN, Wardlaw JM. Use of dynamic contrast-enhanced MRI to measure subtle blood-brain barrier abnormalities. Magn Reson Imaging. 2011; 29:305–314. [PubMed: 21030178]

Barnes SR, Ng TS, Montagne A, Law M, Zlokovic BV, Jacobs RE. Optimal acquisition and modeling parameters for accurate assessment of low Ktrans blood-brain barrier permeability using dynamic contrast-enhanced MRI. Magn Reson Med. 2016; 75:1967–1977. [PubMed: 26077645]

Barnes SR, Ng TS, Santa-Maria N, Montagne A, Zlokovic BV, Jacobs RE. ROCKETSHIP: a flexible and modular software tool for the planning, processing and analysis of dynamic MRI studies. BMC Med Imaging. 2015; 15:19. [PubMed: 26076957]

Bergamino M, Bonzano L, Levrero F, Mancardi GL, Roccatagliata L. A review of technical aspects of T1-weighted dynamic contrast-enhanced magnetic resonance imaging (DCE-MRI) in human brain tumors. Phys Med. 2014; 30:635–643. [PubMed: 24793824]

Bleicher AG, Kanal E. Assessment of adverse reaction rates to a newly approved MRI contrast agent: review of 23,553 administrations of gadobenate dimeglumine. AJR Am J Roentgenol. 2008; 191:W307–311. [PubMed: 19020220]

Bowman GL, Kaye JA, Quinn JF. Dyslipidemia and blood-brain barrier integrity in Alzheimer's disease. Current gerontology and geriatrics research. 2012; 2012

Bronge L, Wahlund L-O. White matter lesions in dementia: an MRI study on blood-brain barrier dysfunction. Dementia and geriatric cognitive disorders. 2000; 11:263–267. [PubMed: 10940677]

Brookes JA, Redpath TW, Gilbert FJ, Murray AD, Staff RT. Accuracy of T1 measurement in dynamic contrast-enhanced breast MRI using two-and three-dimensional variable flip angle fast low-angle shot. Journal of Magnetic Resonance Imaging. 1999; 9:163–171. [PubMed: 10077009]

Brooks WM, Wesley MH, Kodituwakku PW, Garry PJ, Rosenberg GA. 1H-MRS differentiates white matter hyperintensities in subcortical arteriosclerotic encephalopathy from those in normal elderly. Stroke. 1997; 28:1940–1943. [PubMed: 9341699]

Cohen J. A power primer. Psychol Bull. 1992; 112:155–159. [PubMed: 19565683]

Cramer SP, Larsson HB. Accurate determination of blood-brain barrier permeability using dynamic contrast-enhanced T1-weighted MRI: a simulation and in vivo study on healthy subjects and multiple sclerosis patients. J Cereb Blood Flow Metab. 2014; 34:1655–1665. [PubMed: 25074746]

Deoni SC. High-resolution T1 mapping of the brain at 3T with driven equilibrium single pulse observation of T1 with high-speed incorporation of RF field inhomogeneities (DESPOT1-HIFI). Journal of Magnetic Resonance Imaging. 2007; 26:1106–1111. [PubMed: 17896356]

Farrall AJ, Wardlaw JM. Blood-brain barrier: ageing and microvascular disease--systematic review and meta-analysis. Neurobiol Aging. 2009; 30:337–352. [PubMed: 17869382]

Fernando MS, Simpson JE, Matthews F, Brayne C, Lewis CE, Barber R, Kalaria RN, Forster G, Esteves F, Wharton SB, Shaw PJ, O'Brien JT, Ince PG, Function MRCC. Ageing Neuropathology Study, G. White matter lesions in an unselected cohort of the elderly: molecular pathology suggests origin from chronic hypoperfusion injury. Stroke. 2006; 37:1391–1398. [PubMed: 16627790]

Frölich L, Kornhuber J, Ihl R, Fritze J, Maurer K, Riederer P. Integrity of the blood-CSF barrier in dementia of Alzheimer type: CSF/serum ratios of albumin and IgG. European archives of psychiatry and clinical neuroscience. 1991; 240:363–366. [PubMed: 1831668]

Hanyu H, Asano T, Tanaka Y, Iwamoto T, Takasaki M, Abe K. Increased blood-brain barrier permeability in white matter lesions of Binswanger's disease evaluated by contrast-enhanced MRI. Dementia and geriatric cognitive disorders. 2002; 14:1–6. [PubMed: 12053125]

Hartz AM, Bauer B, Soldner EL, Wolf A, Boy S, Backhaus R, Mihaljevic I, Bogdahn U, Klunemann HH, Schuierer G, Schlachetzki F. Amyloid-beta contributes to blood-brain barrier leakage in transgenic human amyloid precursor protein mice and in humans with cerebral amyloid angiopathy. Stroke. 2012; 43:514–523. [PubMed: 22116809]

Hawkins BT, Davis TP. The blood-brain barrier/neurovascular unit in health and disease. Pharmacol Rev. 2005; 57:173–185. [PubMed: 15914466]

Heiss WD, Rosenberg GA, Thiel A, Berlot R, de Reuck J. Neuroimaging in vascular cognitive impairment: a state-of-the-art review. BMC Med. 2016; 14:174. [PubMed: 27806705]

Heye AK, Culling RD, Valdes Hernandez Mdel C, Thrippleton MJ, Wardlaw JM. Assessment of blood-brain barrier disruption using dynamic contrast-enhanced MRI. A systematic review. Neuroimage Clin. 2014; 6:262–274. [PubMed: 25379439]

Heye AK, Thrippleton MJ, Armitage PA, Valdes Hernandez Mdel C, Makin SD, Glatz A, Sakka E, Wardlaw JM. Tracer kinetic modelling for DCE-MRI quantification of subtle blood-brain barrier permeability. Neuroimage. 2016; 125:446–455. [PubMed: 26477653]

Huisa BN, Caprihan A, Thompson J, Prestopnik J, Qualls CR, Rosenberg GA. Long-Term Blood-Brain Barrier Permeability Changes in Binswanger Disease. Stroke. 2015; 46:2413–2418. [PubMed: 26205374]

Iadecola C. Dangerous leaks: blood-brain barrier woes in the aging hippocampus. Neuron. 2015; 85:231–233. [PubMed: 25611503]

Jelescu IO, Leppert IR, Narayanan S, Araujo D, Arnold DL, Pike GB. Dual-temporal resolution dynamic contrast-enhanced MRI protocol for blood-brain barrier permeability measurement in enhancing multiple sclerosis lesions. J Magn Reson Imaging. 2011; 33:1291–1300. [PubMed: 21590997]

Johnson G, Wetzel SG, Cha S, Babb J, Tofts PS. Measuring blood volume and vascular transfer constant from dynamic, T(2)*-weighted contrast-enhanced MRI. Magn Reson Med. 2004; 51:961–968. [PubMed: 15122678]

Kanal E, Tweedle MF. Residual or retained gadolinium: practical implications for radiologists and our patients. Radiology. 2015; 275:630–634. [PubMed: 25942418]

Larsson H, Frederiksen J, Kjaer L, Henriksen O, Olesen J. In vivo determination of T1 and T2 in the brain of patients with severe but stable multiple sclerosis. Magnetic resonance in medicine. 1988; 7:43–55. [PubMed: 3386521]

Lavini C, Verhoeff JJ. Reproducibility of the gadolinium concentration measurements and of the fitting parameters of the vascular input function in the superior sagittal sinus in a patient population. Magn Reson Imaging. 2010; 28:1420–1430. [PubMed: 20817379]

Li KL, Zhu X, Zhao S, Jackson A. Blood-brain barrier permeability of normal-appearing white matter in patients with vestibular schwannoma: A new hybrid approach for analysis of T1 -W DCE-MRI. J Magn Reson Imaging. 2017; 46:79–93. [PubMed: 28117925]

Maillard P, Carmichael O, Harvey D, Fletcher E, Reed B, Mungas D, DeCarli C. FLAIR and diffusion MRI signals are independent predictors of white matter hyperintensities. American Journal of Neuroradiology. 2013; 34:54–61. [PubMed: 22700749]

Maillard P, Mitchell GF, Himali JJ, Beiser A, Fletcher E, Tsao CW, Pase MP, Satizabal CL, Vasan RS, Seshadri S, DeCarli C. Aortic Stiffness, Increased White Matter Free Water, and Altered Microstructural Integrity: A Continuum of Injury. Stroke. 2017; 48:1567–1573. [PubMed: 28473633]

Mecocci P, Parnetti L, Reboldi G, Santucci C, Gaiti A, Ferri C, Gernini I, Romagnoli M, Cadini D, Senin U. Blood-brain-barrier in a geriatric population: Barrier function in degenerative and vascular dementias. Acta Neurol Scand. 1991; 84:210–213. [PubMed: 1950463]

Minoshima S, Giordani B, Berent S, Frey KA, Foster NL, Kuhl DE. Metabolic reduction in the posterior cingulate cortex in very early Alzheimer's disease. Ann Neurol. 1997; 42:85–94. [PubMed: 9225689]

Montagne A, Barnes SR, Sweeney MD, Halliday MR, Sagare AP, Zhao Z, Toga AW, Jacobs RE, Liu CY, Amezcua L, Harrington MG, Chui HC, Law M, Zlokovic BV. Blood-brain barrier breakdown in the aging human hippocampus. Neuron. 2015; 85:296–302. [PubMed: 25611508]

Montagne A, Nation DA, Pa J, Sweeney MD, Toga AW, Zlokovic BV. Brain imaging of neurovascular dysfunction in Alzheimer's disease. Acta Neuropathol. 2016a; 131:687–707. [PubMed: 27038189]

Montagne A, Toga AW, Zlokovic BV. Blood-Brain Barrier Permeability and Gadolinium: Benefits and Potential Pitfalls in Research. JAMA Neurol. 2016b; 73:13–14. [PubMed: 26524294]

Munoz Maniega S, Chappell FM, Valdes Hernandez MC, Armitage PA, Makin SD, Heye AK, Thrippleton MJ, Sakka E, Shuler K, Dennis MS, Wardlaw JM. Integrity of normal-appearing white matter: Influence of age, visible lesion burden and hypertension in patients with small-vessel disease. J Cereb Blood Flow Metab. 2017; 37:644–656. [PubMed: 26933133]

Nelson AR, Sweeney MD, Sagare AP, Zlokovic BV. Neurovascular dysfunction and neurodegeneration in dementia and Alzheimer's disease. Biochim Biophys Acta. 2016; 1862:887–900. [PubMed: 26705676]

Palomares JA, Tummala S, Wang DJ, Park B, Woo MA, Kang DW, St Lawrence KS, Harper RM, Kumar R. Water Exchange across the Blood-Brain Barrier in Obstructive Sleep Apnea: An MRI Diffusion-Weighted Pseudo-Continuous Arterial Spin Labeling Study. J Neuroimaging. 2015; 25:900–905. [PubMed: 26333175]

Patlak CS, Blasberg RG. Graphical evaluation of blood-to-brain transfer constants from multiple-time uptake data. Generalizations. Journal of Cerebral Blood Flow & Metabolism. 1985; 5:584–590. [PubMed: 4055928]

Rosenberg GA. Blood-Brain Barrier Permeability in Aging and Alzheimer's Disease. J Prev Alzheimers Dis. 2014; 1:138–139. [PubMed: 26301207]

Rosenberg GA, Prestopnik J, Adair JC, Huisa BN, Knoefel J, Caprihan A, Gasparovic C, Thompson J, Erhardt EB, Schrader R. Validation of biomarkers in subcortical ischaemic vascular disease of the Binswanger type: approach to targeted treatment trials. J Neurol Neurosurg Psychiatry. 2015; 86:1324–1330. [PubMed: 25618903]

Schabel MC, Parker DL. Uncertainty and bias in contrast concentration measurements using spoiled gradient echo pulse sequences. Phys Med Biol. 2008; 53:2345. [PubMed: 18421121]

Schlageter NL, Carson RE, Rapoport SI. Examination of Blood—Brain Barrier Permeability in Dementia of the Alzheimer Type with [68Ga] EDTA and Positron Emission Tomography. Journal of Cerebral Blood Flow & Metabolism. 1987; 7:1–8. [PubMed: 3100543]

Shah NJ, Zaitsev M, Steinhoff S, Zilles K. A new method for fast multislice T(1) mapping. Neuroimage. 2001; 14:1175–1185. [PubMed: 11697949]

Shindo H, Haruo H, Shimizu S, Iwamoto T. Blood-brain barrier dysfunction in white matter lesions of elderly patients with dementia. Tokyo Ika Daigaku Zasshi. 2005; 63:395–400.

Snyder HM, Corriveau RA, Craft S, Faber JE, Greenberg SM, Knopman D, Lamb BT, Montine TJ, Nedergaard M, Schaffer CB, Schneider JA, Wellington C, Wilcock DM, Zipfel GJ, Zlokovic B, Bain LJ, Bosetti F, Galis ZS, Koroshetz W, Carrillo MC. Vascular contributions to cognitive impairment and dementia including Alzheimer's disease. Alzheimers Dement. 2015; 11:710–717. [PubMed: 25510382]

Sourbron S, Ingrisch M, Siefert A, Reiser M, Herrmann K. Quantification of cerebral blood flow, cerebral blood volume, and blood-brain-barrier leakage with DCE-MRI. Magn Reson Med. 2009; 62:205–217. [PubMed: 19449435]

Sourbron SP, Buckley DL. Classic models for dynamic contrast-enhanced MRI. NMR Biomed. 2013; 26:1004–1027. [PubMed: 23674304]

St Lawrence KS, Owen D, Wang DJ. A two-stage approach for measuring vascular water exchange and arterial transit time by diffusion-weighted perfusion MRI. Magn Reson Med. 2012; 67:1275–1284. [PubMed: 21858870]

Starr J, Wardlaw J, Ferguson K, MacLullich A, Deary I, Marshall I. Increased blood–brain barrier permeability in type II diabetes demonstrated by gadolinium magnetic resonance imaging. Journal of Neurology, Neurosurgery & Psychiatry. 2003; 74:70–76.

Starr JM, Farrall AJ, Armitage P, McGurn B, Wardlaw J. Blood-brain barrier permeability in Alzheimer's disease: a case-control MRI study. Psychiatry Res. 2009; 171:232–241. [PubMed: 19211227]

Taheri S, Gasparovic C, Huisa BN, Adair JC, Edmonds E, Prestopnik J, Grossetete M, Shah NJ, Wills J, Qualls C, Rosenberg GA. Blood-brain barrier permeability abnormalities in vascular cognitive impairment. Stroke. 2011a; 42:2158–2163. [PubMed: 21719768]

Taheri S, Gasparovic C, Shah NJ, Rosenberg GA. Quantitative measurement of blood-brain barrier permeability in human using dynamic contrast-enhanced MRI with fast T1 mapping. Magn Reson Med. 2011b; 65:1036–1042. [PubMed: 21413067]

Tiwari YV, Lu J, Shen Q, Cerqueira B, Duong TQ. Magnetic resonance imaging of blood-brain barrier permeability in ischemic stroke using diffusion-weighted arterial spin labeling in rats. J Cereb Blood Flow Metab. 2017; 37:2706–2715. [PubMed: 27742887]

Tofts PS, Brix G, Buckley DL, Evelhoch JL, Henderson E, Knopp MV, Larsson HB, Lee T-Y, Mayr NA, Parker GJ. Estimating kinetic parameters from dynamic contrast-enhanced T 1-weighted MRI of a diffusable tracer: standardized quantities and symbols. Journal of Magnetic Resonance Imaging. 1999a; 10:223–232. [PubMed: 10508281]

Tofts PS, Brix G, Buckley DL, Evelhoch JL, Henderson E, Knopp MV, Larsson HB, Lee TY, Mayr NA, Parker GJ, Port RE, Taylor J, Weisskoff RM. Estimating kinetic parameters from dynamic contrast-enhanced T(1)-weighted MRI of a diffusable tracer: standardized quantities and symbols. J Magn Reson Imaging. 1999b; 10:223–232. [PubMed: 10508281]

Tomimoto H, Akiguchi I, Suenaga T, Nishimura M, Wakita H, Nakamura S, Kimura J. Alterations of the blood-brain barrier and glial cells in white-matter lesions in cerebrovascular and Alzheimer's disease patients. Stroke. 1996; 27:2069–2074. [PubMed: 8898818]

Ujiie M, Dickstein DL, Carlow DA, Jefferies WA. Blood–brain barrier permeability precedes senile plaque formation in an Alzheimer disease model. Microcirculation. 2003; 10:463–470. [PubMed: 14745459]

van de Haar HJ, Burgmans S, Hofman PA, Verhey FR, Jansen JF, Backes WH. Blood-brain barrier impairment in dementia: current and future in vivo assessments. Neurosci Biobehav Rev. 2015; 49:71–81. [PubMed: 25524876]

van de Haar HJ, Burgmans S, Jansen JF, van Osch MJ, van Buchem MA, Muller M, Hofman PA, Verhey FR, Backes WH. Blood-brain barrier leakage in patients with early Alzheimer disease. Radiology. 2016a; 281:527–535. [PubMed: 27243267]

van de Haar HJ, Jansen JF, van Osch MJ, van Buchem MA, Muller M, Wong SM, Hofman PA, Burgmans S, Verhey FR, Backes WH. Neurovascular unit impairment in early Alzheimer's disease

measured with magnetic resonance imaging. Neurobiol Aging. 2016b; 45:190–196. [PubMed: 27459939]

van de Haar HJ, Jansen JFA, Jeukens C, Burgmans S, van Buchem MA, Muller M, Hofman PAM, Verhey FRJ, van Osch MJP, Backes WH. Subtle blood-brain barrier leakage rate and spatial extent: considerations for dynamic contrast-enhanced MRI. Med Phys. 2017

Varatharaj A, Galea I. The blood-brain barrier in systemic inflammation. Brain Behav Immun. 2017; 60:1–12. [PubMed: 26995317]

Wang H, Golob EJ, Su MY. Vascular volume and blood-brain barrier permeability measured by dynamic contrast enhanced MRI in hippocampus and cerebellum of patients with MCI and normal controls. Journal of Magnetic Resonance Imaging. 2006; 24:695–700. [PubMed: 16878309]

Wang J, Fernandez-Seara MA, Wang S, St Lawrence KS. When perfusion meets diffusion: in vivo measurement of water permeability in human brain. J Cereb Blood Flow Metab. 2007; 27:839–849. [PubMed: 16969383]

Wardlaw JM, Doubal FN, Valdes-Hernandez M, Wang X, Chappell FM, Shuler K, Armitage PA, Carpenter TC, Dennis MS. Blood-brain barrier permeability and long-term clinical and imaging outcomes in cerebral small vessel disease. Stroke. 2013; 44:525–527. [PubMed: 23233386]

Wardlaw JM, Valdes Hernandez MC, Munoz-Maniega S. What are white matter hyperintensities made of? Relevance to vascular cognitive impairment. J Am Heart Assoc. 2015; 4:001140. [PubMed: 26104658]

Weaver J, Jalal FY, Yang Y, Thompson J, Rosenberg GA, Liu KJ. Tissue oxygen is reduced in white matter of spontaneously hypertensive-stroke prone rats: a longitudinal study with electron paramagnetic resonance. Journal of Cerebral Blood Flow & Metabolism. 2014; 34:890–896. [PubMed: 24549186]

Wisniewski H, Kozlowski P. Evidence for Blood-Brain Barrier Changes in Senile Dementia of the Alzheimer Type (SDAT). Ann N Y Acad Sci. 1982; 396:119–129. [PubMed: 6185032]

Wong SM, Jansen JF, Zhang CE, Staals J, Hofman PA, van Oostenbrugge RJ, Jeukens CR, Backes WH. Measuring subtle leakage of the blood-brain barrier in cerebrovascular disease with DCE-MRI: Test-retest reproducibility and its influencing factors. J Magn Reson Imaging. 2017

Zenaro E, Piacentino G, Constantin G. The blood-brain barrier in Alzheimer's disease. Neurobiol Dis. 2017; 107:41–56. [PubMed: 27425887]

Zhang CE, Wong SM, van de Haar HJ, Staals J, Jansen JF, Jeukens CR, Hofman PA, van Oostenbrugge RJ, Backes WH. Blood–brain barrier leakage is more widespread in patients with cerebral small vessel disease. Neurology. 2017; 88:426–432. [PubMed: 28031395]

Zipser B, Johanson C, Gonzalez L, Berzin T, Tavares R, Hulette C, Vitek M, Hovanesian V, Stopa E. Microvascular injury and blood–brain barrier leakage in Alzheimer's disease. Neurobiol Aging. 2007; 28:977–986. [PubMed: 16782234]

Highlights

- We examine the challenges in measuring subtle Blood-Brain Barrier changes and review DCE-MRI studies of BBB breakdown in dementia.
- A systematic review comparing methodologies from recent in-vivo MRI studies is presented with the focus on finding the optimal technique.
- The reported BBB permeability values in dementia are compared across different studies and across various brain regions.
- We conclude that reliable measurement of low-level BBB permeability across sites remains a difficult problem and a standardization of the methodology for both data acquisition and quantitative analysis is required.

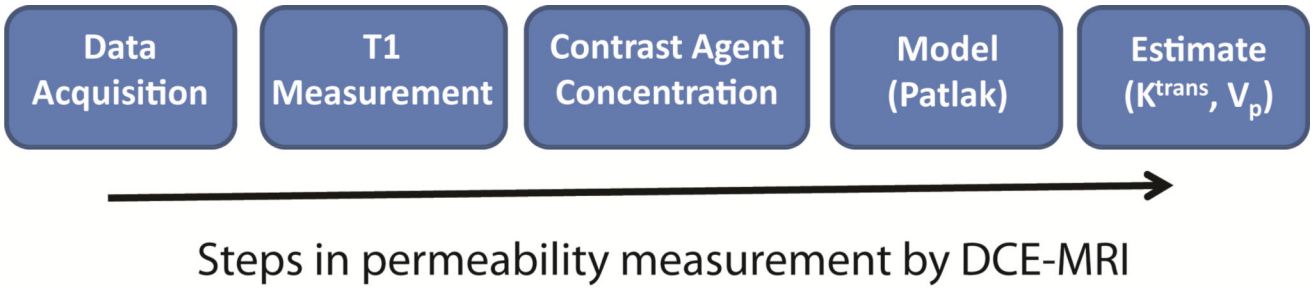

Figure 1.

The DCE-MRI method consists of five steps. During data acquisition we choose the contrast agent (CA) type and dosage and the MRI sequence for T1 mapping. T1 and CA concentrations are then calculated from the data. Next we have to make a choice of the tracer-kinetic model to use. Patlak model is one such example. The model parameters are finally calculated.

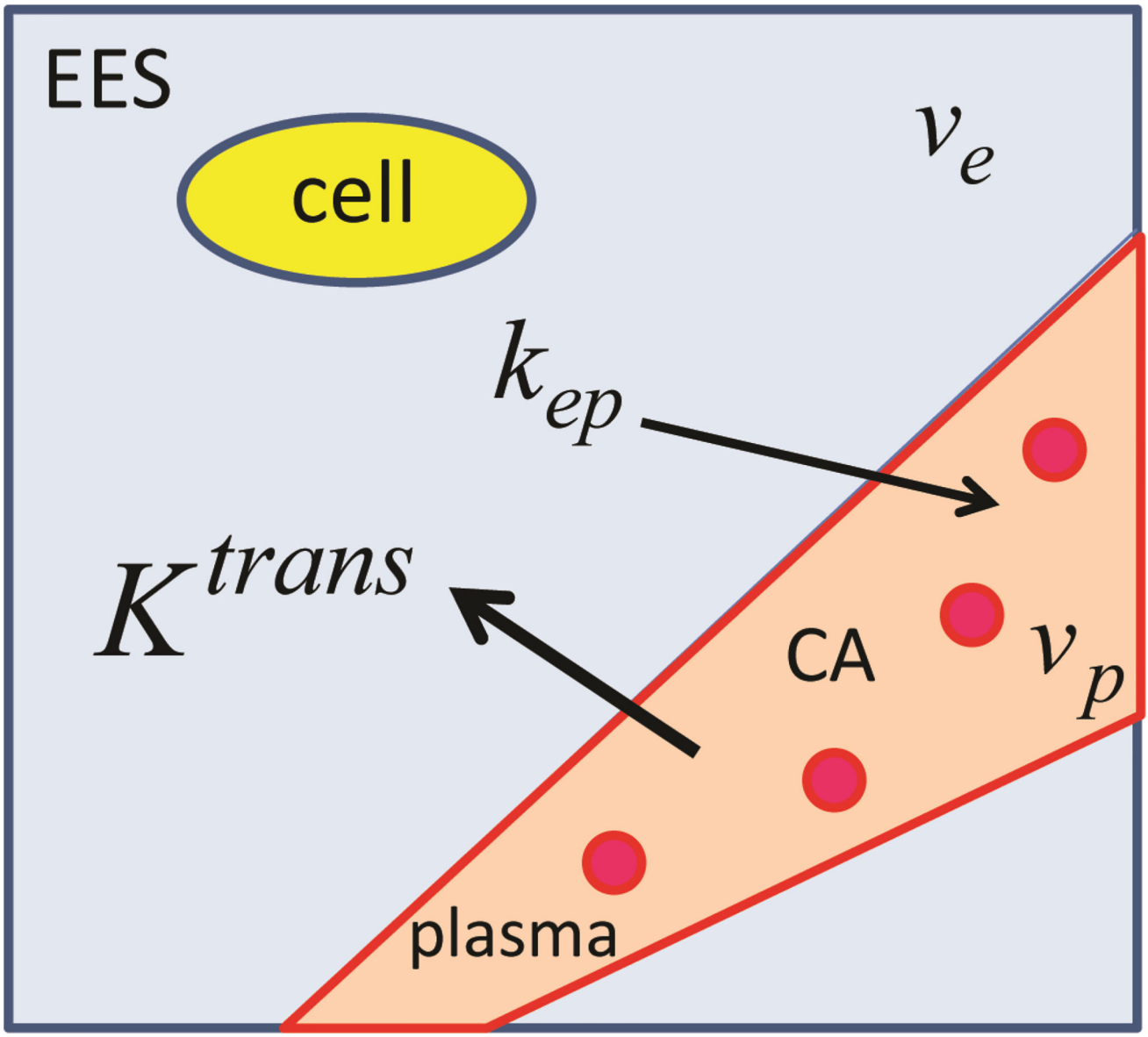

Figure 2.

The tissue model within a voxel is described for the tracer-kinetic model described by Equation [1]. The voxel is divided into extravascular extracellular space (EES) with a volume fraction v_e (blue), and the intravascular space (light red). The EES space excludes the brain cells (yellow) and the plasma (light red) with volume fraction v_p excludes the blood cells (red). The model parameters to be estimated are volume transfer constant K^{trans}, rate constant for back flow k_{ep}, and the volume fractions v_p and v_e.

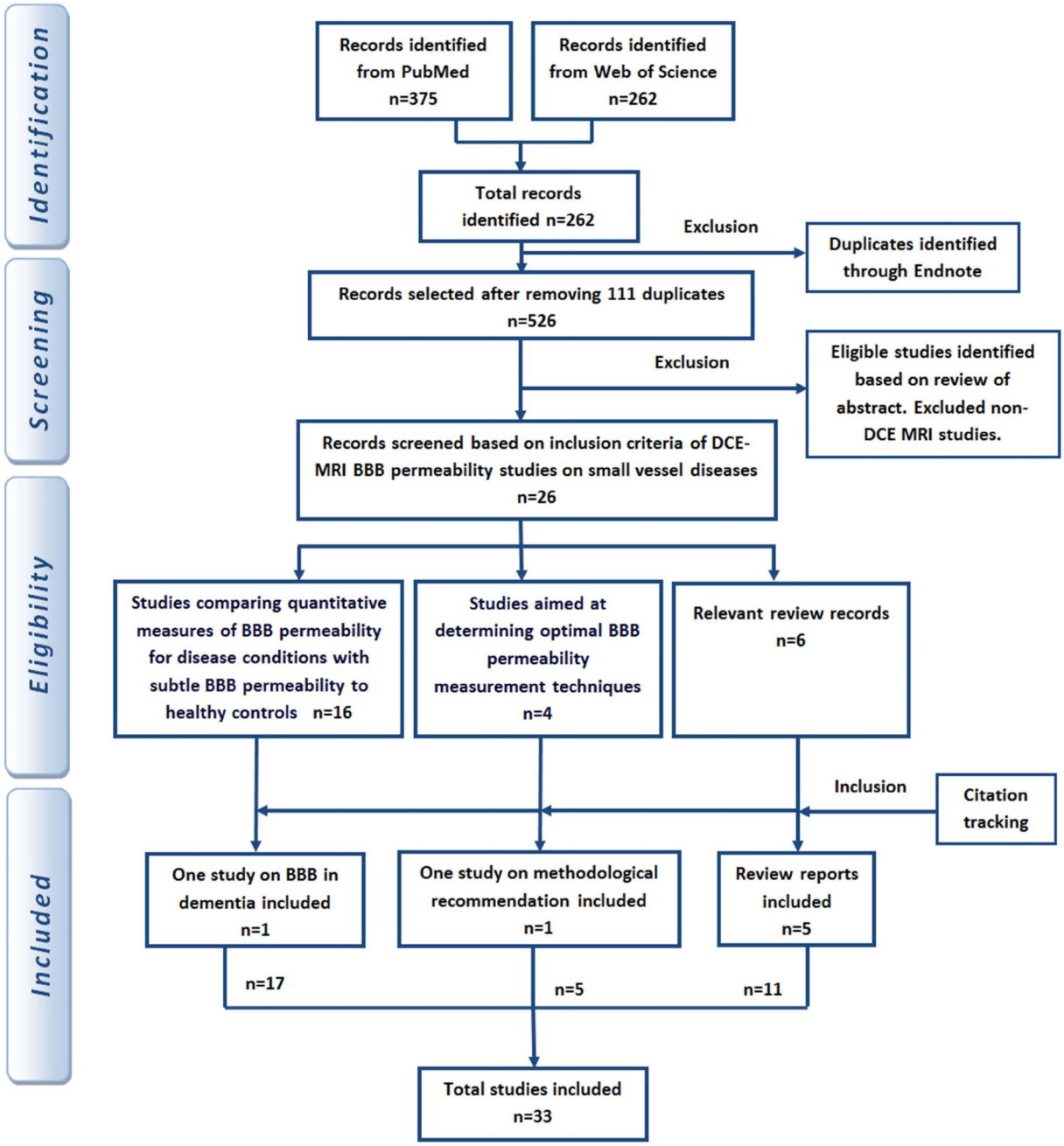

Figure 3.
The flow diagram summarizes the search strategy and inclusion-exclusion criteria.

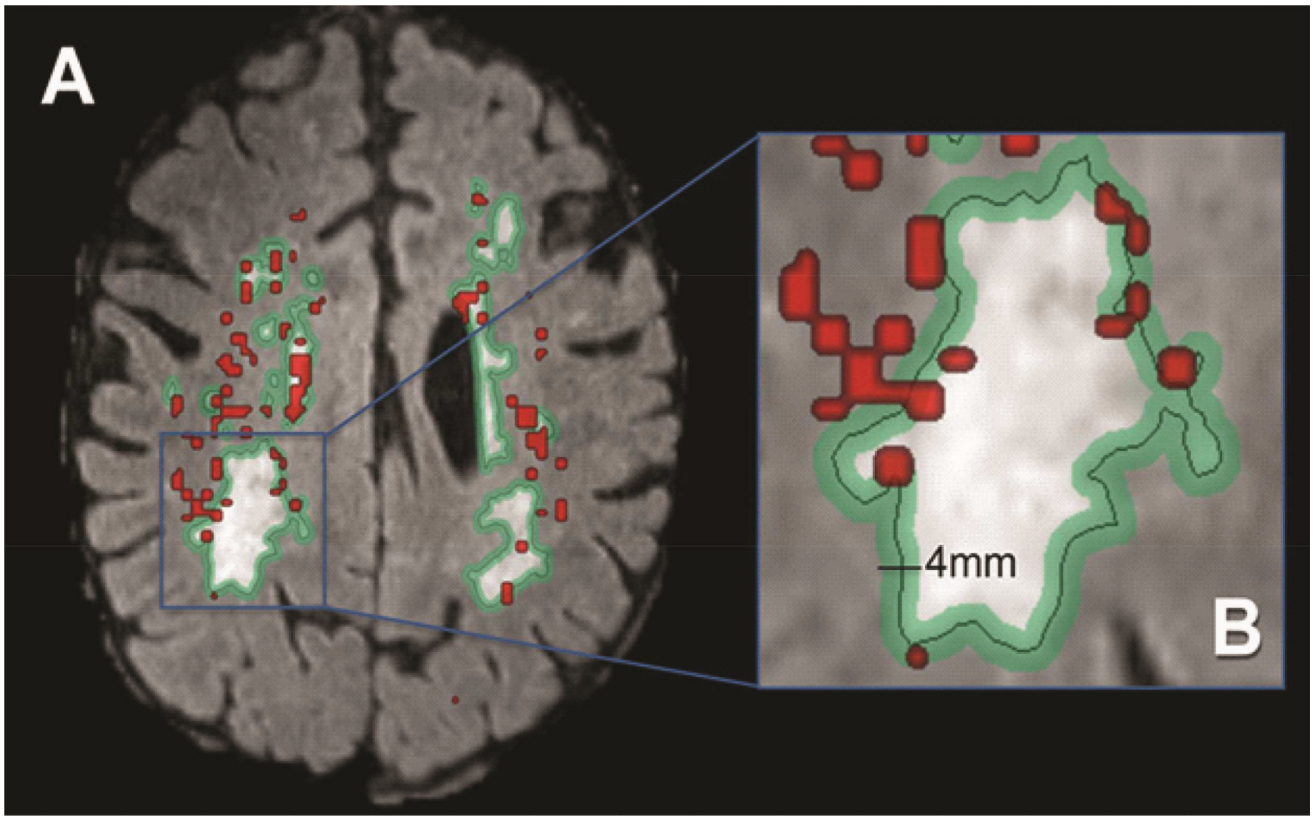

Figure 4.

A majority of increased permeability (red) is within a penumbra (green) marked around the white matter hyper-intensity. Image (B) is an enlarged version of the image (A).

Table 1

Comparison of DCE-MRI Studies on diseases with subtle BBB permeability

Disease Group	Study (Reference)	Sample Size C/P	Mean Age C/P	DCE-MRI Protocol FS/ST/PS	CA/Dose (mmol/kg)	Quantity measured	Brain regions
SVD	(Wardlaw et al., 2013)	NA/97	NA/65	1.5T/30m/FSPGR	Gd-DTPA/40 *	$Slope_{sec}$	WMH NAWM
	(Wong et al., 2017)	NA/16	NA/66	3T/1.33/22.5m DSRGRE	Gadobutrol/0.1	K^{trans}, v_p	WM,GM
	(Zhang et al., 2017)	39/77	69/70	3T/1.5/25m DSRGRE	Gadobutrol/0.1	K^{trans}, v_p	WM,GM
	(Munoz Maniega et al., 2017)	NA/199	NA/66	1.5T/24m/FSPGR	Gd-DOTA/0.1	$Slope_{sec}$	WMH NAWM
Dementia	(Bronge and Wahlund, 2000)	55	72/73	1.5T/25m/GE/SE	GdDTPA-BMA/0.2	SER	WMLs
	(Shindo et al., 2005)	14/21	78/79	15m	Gd-DTPA	T1 signal change	WMLs
AD	(Starr et al., 2009)	15/15	73/74	1.5T/30m/FSPGR	Gd-DTPA/20 *	SER	WM,GM CSF
	(van de Haar et al., 2016a)	17/16	76/74	3T/1.5/25m DSRGRE	Gadobutrol/0.1	K^{trans}, v_p	WM,GM
	(van de Haar et al., 2016b)	16/14	76/73	3T/1.5/25m DSRGRE	Gadobutrol/0.1	K^{trans}, v_p	WM,GM
BD	(Hanyu et al., 2002)	27/14	77/78	15m	Gd-DTPA	T1 signal change	WMLs
	(Huisa et al., 2015)	12/22	61/67	1.5T/22.5m/TAPIR	Gd-DTPA/0.025	K^{trans}	WM
	(Rosenberg et al., 2015)	20/62	44/66	1.5T/22.5m/TAPIR	Gd-DTPA/0.025	K^{trans}	WM
VCI	(Taheri et al., 2011a)	17/60	44/63	1.5T/22.5m/TAPIR	Gd-DTPA/0.025	K^{trans}	WM
	(Taheri et al., 2011b)	20/45	51/64	1.5T/22.5m/TAPIR	Gd-DTPA/0.025	K^{trans}	WM
MCI	(Wang et al., 2006)	10/11	74/74	1.5T/6.8m/3DGE	GdDTPA-BMA/1 **	SER	HC Cerebellem
Diabetes	(Starr et al., 2003)	10/10	68/68	1.9T/90m/FLAIR	Gd-DTPA/0.2	SER	WM,GM
Aging/MCI/MS	(Montagne et al., 2015)	24/40	55/55	3T/16m/SPGR	Gd-DTPA/0.05	K^{trans}	HC,GM WM

SVD, Small Vessel Disease; AD, Alzheimer's Disease; BD, Binswanger's Disease; VCI, Vascular Cognitive Impairment; MCI, Mild Cognitive Impairment; MS, Multiple Sclerosis; C, Controls; P, Patients; FS, Field Strength; PS, Pulse Sequence; ST, Scan Time; CA, Contrast Agent; GE, Gradient Echo; SE, Spin Echo; WMLs, White Matter Lesions; ROI, Region of Interest; WM, White Matter; GM, Gray Matter; HC, Hippocampus; FSPGR, Fast Spoiled Gradient Recalled Echo; CSF, Cerebro-Spinal Fluid; TAPIR, T1-mapping with partial inversion recovery; SER, Signal Enhancement Ratio; $Slope_{sec}$, Slope of signal enhancement curve; DSRGRE, Dual resolution Saturation Recovery Gradient Recalled Echo, NA, Not applicable to the study.

* denotes CA dosage expressed in ml

** denotes CA dosage expressed in ml/10 lb of body weight

Table 2

A comparison of K^{trans} values in controls across different research groups. The missing values were not reported in the studies reviewed.

Groups	Study	Controls K^{trans} ($\times 10^{-3}$ min^{-1})	
		WM	GM
Backes	(van de Haar et al., 2017)	0.070±0.06	0.008±0.076(CGM)
	(Zhang et al., 2017)	1.05±0.05	1.49±0.07(CGM), 1.11±0.06(DGM)
	(van de Haar et al., 2016a)	0.070±0.06	0.017±0.08
	(van de Haar et al., 2016b)		0.18±0.13
Zlokovic	(Barnes et al., 2016)	2.25±0.25	3±1
	(Montagne et al., 2015)	2.19±0.18	0.81±0.17(Thalamus)
Rosenberg	(Taheri et al., 2011a)	1.5±0.5	
	(Taheri et al., 2011b)	1.8±0.15	

WM, White Matter; GM, Gray Matter; CGM, Cortical Gray Matter; DGM, Deep Gray Matter

Table 3

A comparison of K^{trans} values in different patient disease categories across different research groups. The missing values were not reported in the studies reviewed.

Groups	Study	Disease	Patients K^{trans} ($\times 10^{-3}$ min^{-1})			
			NAWM	WM	GM	WMH
Backes	(van de Haar et al., 2017)	early AD	0.075±0.046		0.104±0.124	
	(Zhang et al., 2017)	cSVD	0.97±0.04		1.43±0.05(CGM) 1.06±0.04(DGM)	0.85±0.03
	(van de Haar et al., 2016a)	early AD	0.065±0.043	0.066±0.04	0.089±0.11	0.106±0.11
	(Wong et al., 2017)	cSVD		1.3±0.5	2.2±0.7	
	(van de Haar et al., 2016b)	early AD			0.27±0.14	
Wardlaw	(Munoz Maniega et al., 2017)	Mild stroke	0.224±0.37			0.350±0.48
	(Heye et al., 2016)	Mild stroke	0.296±0.01		0.391±0.012 (DGM)	0.396±0.013
Zlokovic	(Montagne et al., 2015)	MCI		2.30±0.36	0.89±0.24 *	
		MS		2.53±0.27	0.80±0.16 *	
Rosenberg	(Taheri et al., 2011a)	SIVD				3±2
		MI/LAC				2.5±1
	(Taheri et al., 2011b)	VCI		2.4±0.5		
		MS		2.3±0.5		

*, denotes thalamus regions

cSVD, Cerebral Small Vessel Disease; AD, Alzheimer's Disease; VCI, Vascular Cognitive Impairment; MCI, Mild Cognitive Impairment; MS, Multiple Sclerosis; WMH, White Matter Hyperintensities; WM, White Matter; GM, Gray Matter; NAWM, Normal Appearing White Matter; SIVD, Subcortical Ischemic Vascular Disease; MI/LAC, Multiple and Lacunar infarcts

Table 4

Comparison of Studies on finding optimal DCE-MRI methodology for subtle BBB permeability. The missing entries were not discussed in the reviewed study.

Factors considered	Armitage et al., 2011)	Cramer and Larsson, 2014)	Barnes et al., 2016)	Heye et al., 2016)	van de Haar et al., 2017)
T1 mapping					
T1 mapping method used?	SPGR	SRGE	SPGR	SPGR	DSRGE
T1 mapping methods compared?	No	No	No	No	No
Contrast agent					
Contrast agent used	Gadodiamide	Gadovist,	Gd-DTPA	Gd-DOTA	Gadobutrol
CA dosage used	40 ml	0.045 mmol/kg	0.05 mmol/kg	0.1 mmol/kg	0.1 mmol/kg
CA dosage varied.	No	No	No	No	No
Acquisition factors					
Scanner type	1.5T/GE	3T/Phillips	3T/GE	1.5T/GE	3T/Phillips
Scanner Drift	Yes	Yes	Yes	Yes	No
Scanner Noise	Yes	No	No	No	No
Temporal Resolution	No	Yes	Yes	Yes	Yes
Spatial Resolution	No	No	No	Yes	No
Baseline measurements	2	No	Yes	No	No
Experiment duration	No	Yes	Yes	No	Yes *
Model Selection					
Methods to choose optimal model studied?	No	Yes	Yes	Yes	No
Did the study involve real data and simulations?	Yes	Yes	Yes	Yes	Yes
Optimal Recommendations					
Pulse sequence	NS	NS	NS	NS	NS
Contrast agent dosage	NS	NS	NS	NS	NS
Permeability model		Patlak	Patlak	Patlak	
Acquisition duration		15 m	10–30 m		
Baseline scan duration			1–4 min		
Temporal resolution		1.25s	< 60s/image	Low TR	
Spatial resolution				High SR	

TR, temporal resolution; SR, Spatial resolution; SPGR, Spoiled Gradient Recalled Echo; DSRGE, Dual resolution Saturation Recovery Gradient Recalled Echo; NS, Not studied

* - scan duration recommended against different sample sizes and effect sizes

Table 5

Effect sizes calculated for the studies reported on comparing K^{trans} values between controls and patients across different research groups.

$$\textbf{Effect Size} = \frac{\mu_{patient} - \mu_{control}}{s_{pooled}}$$

Groups	Study	Disease	Sample Size		Effect Size	
			Patients	Controls	WM	GM
Backes	(van de Haar et al., 2017)	early AD	16	17	0.09314	0.9404(CGM)
	(Zhang et al., 2017)	cSVD	77	39	−1.83533	−1.04447(CGM) −1.05021(DGM)
	(van de Haar et al., 2016a)	early AD	16	17	−0.07796	0.75237
	(van de Haar et al., 2016b)	early AD	14	16	NA	−0.66798
Zlokovic	(Montagne et al., 2015)	MCI	21	18	0.37743	0.37961(Thalamus)
Rosenberg	(Taheri et al., 2011a)	SIVD	36	17	0.89268	NA
		MI/LAC	17	17	1.26491	NA
	(Taheri et al., 2011b)	VCI	45	20	1.40878	NA

WM, White Matter; GM, Gray Matter; CGM, Cortical Gray Matter; DGM, Deep Gray Matter; cSVD, Cerebral Small Vessel Disease; AD, Alzheimer's Disease; VCI, Vascular Cognitive Impairment; MCI, Mild Cognitive Impairment; SIVD, Subcortical Ischemic Vascular Disease; MI/LAC, Multiple and Lacunar infarcts

NA – Effect sizes not calculated as corresponding K^{trans} values were not reported in the studies reviewed